Multilayer Laue Lenses as High-Resolution X-ray Optics

J. Maser, G. B. Stephenson, S. Vogt, W. Yun, A. Macrander, H. C. Kang, C. Liu, R. Conley.
Argonne National Laboratory, Argonne, IL 60439

Keywords: X-ray Optics, High Resolution Optics, Diffractive Optics, Zone Plates, Multilayers,Volume Holograms.

ABSTRACT

Using Fresnel zone plates, a spatial resolution between 20 nm for soft x-rays and 70 nm for hard x-rays has been achieved. Improvement of the spatial resolution without loss of efficiency is difficult and incremental due to the fabrication challenges posed by the combination of small outermost zone width and high aspect ratios. We describe a novel approach for high-resolution x-ray focusing, a multilayer Laue lens (MLL). The MLL concept is a system of two crossed linear zone plates, manufactured by deposition techniques. The approach involves deposition of a multilayer with a graded period, sectioning it to the appropriate thickness, assembling the sections at the optimum angle, and using it in Laue geometry for focusing. The approach is particularly well suited for high-resolution focusing optics for use at high photon energy. We present a theory of the MLL using dynamic diffraction theory and Fourier optics.

1. INTRODUCTION

Efficient focusing of x-rays to nanometer dimensions using diffractive optics has been limited by the ability to manufacture diffracting structures with small d-spacings and the large thicknesses imposed by the weak interaction of x-rays with matter (Figure 1). To achieve a focal spot size of, e.g., 6 nm at a photon energy of 10 keV with good efficiency, Fresnel zone plates (Fresnel zone plate, FZP) of a heavy material such as gold with an outermost zone width of dr_N = 5 nm and a thickness of t = 2 μm are required. Higher energies require larger thicknesses. For example, a thickness of 6 μm in gold would be required for efficiently focusing at 30 keV, and a thickness of 20 μm at 100 keV. The corresponding aspect ratios $A = t/dr_N$ are 400:1 for 10 keV, 1100:1 for 30 keV, and 4,000:1 for 100 keV.

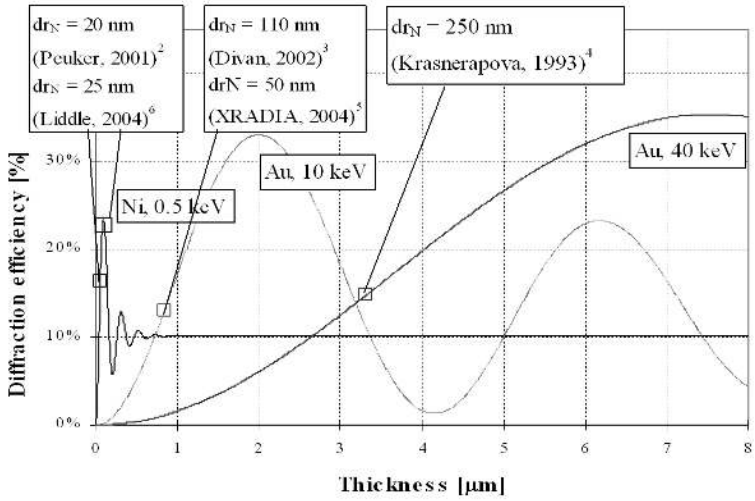

Figure 1: Diffraction efficiency of thin transmission gratings as function of zone plate thickness for x-rays with photon energies from 0.5 – 40 keV. The curves were calculated using a thin-grating approach,[1] and for

Design and Microfabrication of Novel X-Ray Optics II, edited by
Anatoly A. Snigirev, Derrick C. Mancini, Proceedings of SPIE Vol. 5539
(SPIE, Bellingham, WA, 2004) · 0277-786X/04/$15 · doi: 10.1117/12.560046

rectangular grating profile. The smallest outermost zone width manufactured for the respective energy ranges is indicated. The aspect ratios typically achieved are on the order of 6:1 – 15:1. [2,3,4,5,6]

To date, high-resolution zone plates are manufactured using e-beam lithography and consecutive pattern transfer. Typical aspect ratios achieved using this approach are on the order of 7:1 – 15:1.[2,3,4,5,6] In order to achieve small periods and high aspect ratios, we have therefore begun to explore a deposition-based approach to optics manufacturing. Deposition techniques for fabrication of zone plates have been employed previously, typically using a cylindrical wire as the substrate.[7,8,9,10,11] However, to date, this pioneering work has yielded a highest resolution of about 300 nm at 24 keV,[8] in part due to challenges in deposition on a thin wire. We have chosen to deposit the multilayer on a flat substrate, which allows the critical outermost zones to be deposited first, and allows tilting of opposite sides of the structure to the optimum angles. Here, we describe the concept and present theoretical calculations of the performance. Initial experimental results are presented in a companion paper.[12]

2. CONCEPT OF MULTILAYER LAUE LENS

A Multilayer Laue lens (MLL) is a set of multilayers used in transmission (Laue) geometry for focusing (Figure 2). A 1-D MLL, corresponding to a linear zone plate, consists of two sections of multilayers with a graded period that varies in the deposition direction. A 2-D MLL consists of two 1-D MLL's placed in series along the optical axis and oriented perpendicularly with respect to each other. The period variation of each multilayer is given by the zone plate law.[13,14]

$$r_n = \sqrt{n\lambda f + \frac{1}{4}n^2\lambda^2},$$

where r_n is the radius of the n^{th} Fresnel zone, λ the wavelength, and f the focal length in the first diffraction order. The zone width dr_n is the difference of adjacent radii, $dr_n = r_n - r_{n-1}$,

$$dr_n = \frac{\lambda f + \frac{n\lambda^2}{2}}{2r_n},$$

and corresponds to a local period $\Lambda(r_n)$ of the MLL of $\Lambda(r_n) = 2 \cdot dr_n$.

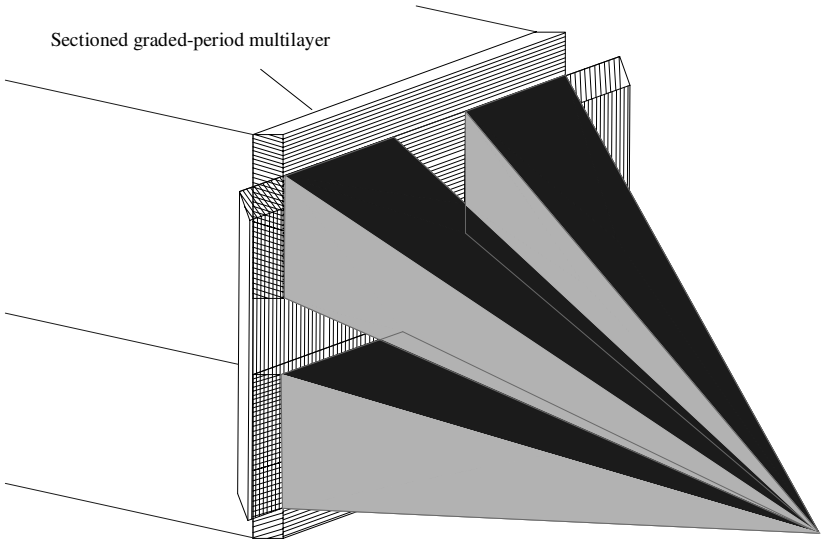

Figure 2: Geometry of a multilayer Laue lens. Two sections of graded-period multilayers are assembled into a 1-D MLL. A second assembly, rotated by 90º, is placed behind the first to provide focusing in the perpendicular direction. A central obstruction blocks undiffracted radiation from reaching the focal plane.

Figure 3 shows the manufacture and assembly of the MLL. A graded-period multilayer is obtained by alternatively depositing two materials, e.g. W and Si, on a flat substrate. Deposition begins with the smallest period, thus minimizing the effect any increase of roughness during deposition has on the focusing properties. The resulting multilayer is sectioned to the thickness optimized for operation at a specific photon energy range. Two sections are then assembled into a 1-D MLL, with the largest periods facing each other. Each section can be tilted with respect to the optical axis by an angle ψ to optimize the efficiency. Two 1-D MLLs are crossed to form a 2-D MLL.

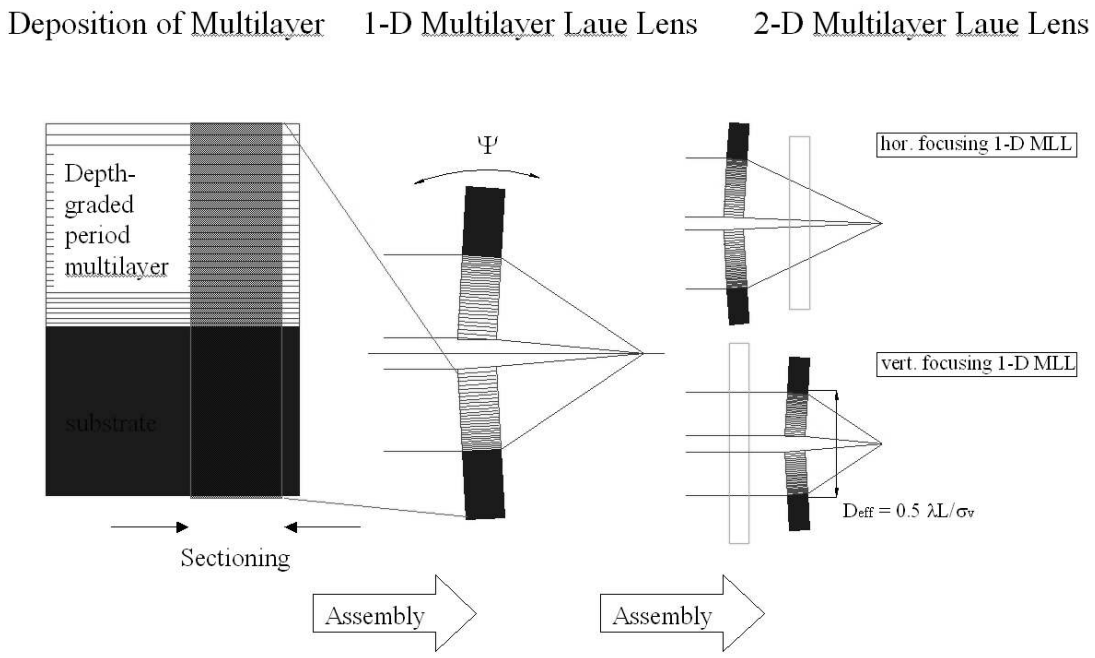

Figure 3: A graded-period multilayer is deposited on a flat substrate, and sectioned to the appropriate thickness. Two thinned sections are assembled into a 1-D MLL. Tilting of an individual section by an angle ψ with respect to the optical axis is required to optimize the efficiency. Two 1-D MLL's are assembled into a 2-D MLL.

Since the two 1-D MLLs have to be placed in series, the system is astigmatic. This can be corrected by fabricating 1-D MLLs with different diameters and matching the lateral coherence length in horizontal and vertical direction to those diameters. In a synchrotron beamline, this can be achieved by matching the effective aperture $D_{eff,\,v}$ of the 1-D MLL to the lateral coherence length in the vertical direction, placing the second 1-D MLL with larger effective aperture $D_{eff,\,h}$ upstream of the first, and using a spatial filter to match the lateral coherence length in the horizontal direction to $D_{eff,\,h}$. The effective aperture of the vertically focusing 1-D MLL is given by $D_{eff,\,v} = 0.5\lambda L/\sigma$, where σ is the FWHM size of the x-ray source and L the distance of the MLL from the source. The effective aperture $D_{eff,\,h}$ of the horizontally focusing zone plate is determined by the distance from the vertically focusing MLL.

Figure 4 compares the geometry of a MLL and a circular FZP with outer zone width dr_N. For the purpose of discussing the acceptance, a symmetric MLL with identical horizontal and vertical effective apertures D_{eff}, and a zone plate with the same diameter is used. The zones in the center of the MLL will not be deposited to provide space for assembly. To prevent undiffracted radiation from reaching the focal plane, a central obstruction of size d_i has to be positioned on the optical axis. The total acceptance of MLL and FZP depends on the size of the central obstruction. The area of the MLL that is available for focusing scales with the area fraction $F_A = (1-d_i/D_{eff})^2$, whereas the area fraction of a zone plate is $F_A = 1- (d_i/D_{eff})^2$. The solid square in figure 4 indicates one of the corner areas of the MLL that contribute diffracted radiation to the focused beam.

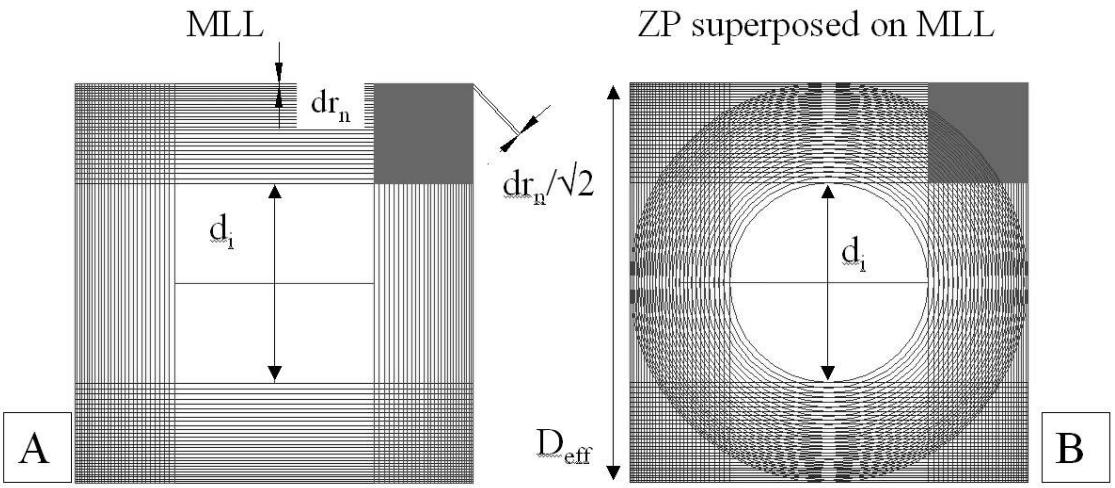

Figure 4: Geometry of a MLL and a FZP. Figure 4A shows a MLL with effective aperture D_{eff}, an outermost zone width dr_n and a central obstruction of size d_i. The filled area on the upper right corresponds to one of 4 MLL areas that contribute to focusing. Figure 4B shows a zone plate of the same effective aperture and central obstruction size superposed on the MLL. It should be noted that (i) the smallest corresponding outermost zone width of a MLL is $1/\sqrt{2}$ of that of a zone plate with the same effective aperture, and that (ii) the effective area of a MLL is significantly smaller than that of the corresponding zone plate as long as the central obstruction is large.

Table 1: Area fraction F_A of a MLL and a FZP vs. the relative size r_A of the central obstruction, as well as the ratio of areas for a MLL and a FZP. For a relative size r_A of 0.25 and smaller, the MLL and FZP have comparable acceptance areas. For central obstructions larger than 0.25, both the acceptance area and the area fraction of the MLL quickly become smaller.

$r_A = d_i/D_{eff}$	0	0.25	0.33	0.5
F_A *(MLL)*	100%	56%	45%	25 %
area(MLL)/area(FZP)	$4/\pi$	0.93	0.89	0.42

Table 2: Parameter for MLLs with outermost zone widths of 5 nm and 2 nm for use at a third-generation synchrotron facility.

Effective Aperture D_{eff}	30 μm			
Material	W/Si			
Photon energy	10 keV		30 keV	
Thickness t	4 μm		10 μm	
Outermost zone width dr_N	5 nm	2 nm	5 nm	2 nm
Focal length f	1.2 mm	0.48 mm	3.6 mm	1.4 mm
Zone number N	1500	3750	1500	3750
Aspect ratio $A = t/dr_N$	800:1	2000:1	2000:1	5000:1

Table 1 lists the area fraction of a MLL and provides a comparison with a FZP. If the ratio r_A of central obstruction and effective diameter, $r_A = d_i/D_{eff}$, is smaller than 0.25, the acceptance of the MLL is comparable to that of the FZP. With increasing size of the central obstruction, the area fraction of the MLL quickly becomes smaller. For example, for $r_A = 0.5$, only 25% of the illuminated MLL area contributes to the focus, whereas 75% of the illuminated area of a zone plate would contribute to the focus. From the perspective of focusing efficiency, i.e., fraction of the incident radiation diffracted into the focal spot, it is therefore important to keep r_A at 0.25 or smaller.

Table 2 lists parameters for a MLL for use at a third-generation synchrotron for different energies. A typical FWHM vertical source size is σ_y = 50 μm, which requires an effective aperture of D_{eff} = 30 μm at a typical distance of 75 m from the source. It should be noted that the zone numbers *N* listed in the table are well suited to use of a crystal monochromator.

3. DIFFRACTION PROPERTIES OF MULTILAYER LAUE LENSES

Diffracting optics such as FZPs and MLLs can be considered as "volume holograms" or "volume gratings". The diffraction properties of volume gratings can be described using a variety of approaches, namely couple mode theory and coupled wave theory.[15,16,17,18] To describe the diffraction properties of a MLL, we use a "locally one-dimensional" version of N-wave coupled wave theory.[19] This approach is well suited to describe both the outer areas of a high-resolution optic, where, similar to diffraction by crystals, only two waves interact, as well as the central area, which may exhibit multi-wave interaction as is commonly found in thin gratings. N-wave coupled wave theory (CWT) applies in particular in the intermediate case, where a small number of diffracted waves is present. If scattering is weak, as is the case for x-rays, and the thickness of the MLL is small compared to the focal length ($t << f$),[20,21] a first-order approach of CWT can be used. Second derivatives of the electrical field are neglected, and refraction at interfaces is taken into account explicitly by using Snell's law.

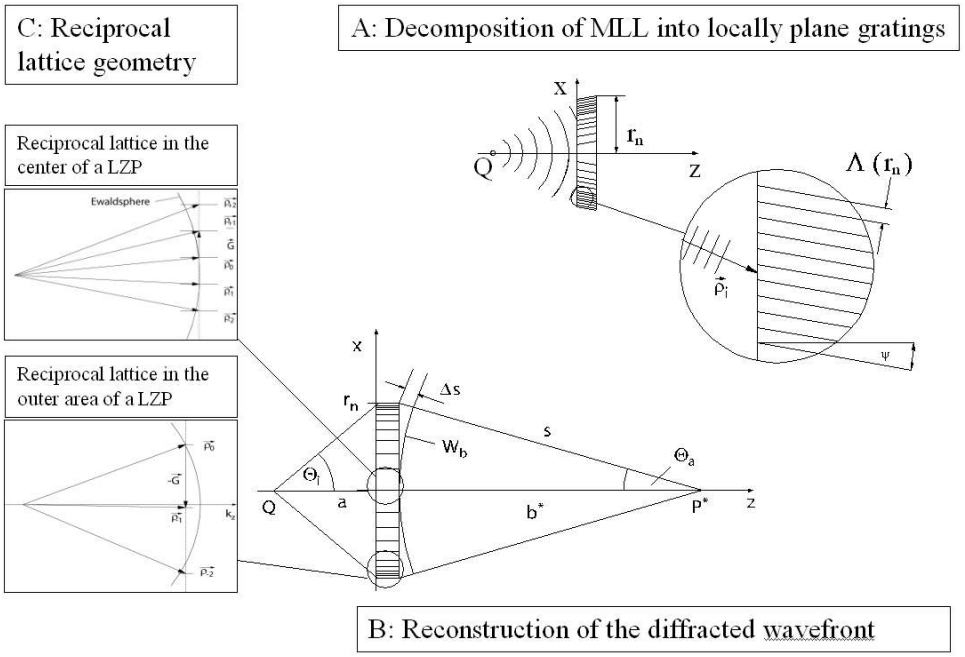

Figure 5: Model for the diffraction of a spherical wave by a MLL with small outermost zone width and high aspect ratio. **A)** The incident cylindrical wave is decomposed into a set of plane waves with radially changing wave vector $\vec{\rho}_i$ and incidence angle θ_i. The MLL is decomposed into local gratings with radially changing d-spacing $\Lambda(r_n) = 2 \cdot dr_n(r_n)$. A "locally one-dimensional" approach of coupled wave theory is used to calculate the complex amplitude $A(t, r_n)$ of the wave field at the rear surface (z=t) of the MLL.
B) The diffracted wave front W_b is reconstructed from the $A(t, r_n)$. The intensity distribution at point P* in the image space is calculated by propagating the wave field to the desired plane through P*. This allows calculation of the point spread function and the modulation transfer function.
C) The diffraction properties change as function of d-spacing and aspect ratio. In the center of the MLL, the d-spacing is relatively large, the reciprocal lattice rods are long in the k_z direction, and the close proximity of the reciprocal lattice allows a significant number of eigenmodes to be excited. As the d-spacing becomes smaller, the diffraction angle increases, and fewer reciprocal lattice rods intersect the Ewald sphere. Accordingly, fewer eigenmodes are excited. At the same time,

deviations from the Bragg condition significantly affect the amplitude and the phase of the eigenmode. To achieve high diffraction efficiency and minimize phase effects, the zones therefore have to be tilted with respect to the optical axis.

Figure 5 illustrates modeling of the MLL in the context of locally one-dimensional CWT: the incident spherical wave front is decomposed into "locally plane" waves with wave vector $\vec{\rho}_i$ and incident angle θ_i, and the MLL is decomposed into "locally plane" gratings with d-spacing $\Lambda(r_n)$ and slanting angle $\psi(r_n)$. After refraction at the incidence surface, the incident wave excites a system of eigenmodes of the local grating with wave vectors $\vec{\rho}_l = \vec{\rho}_i + l\vec{G}$ and complex amplitudes $A_l(t)$. The thickness of the local grating is t. The amplitudes $A_l(t)$ inside the grating yield, after refraction at the rear interface, the local amplitudes $A^*(r_n, t)$ on the rear surface of the MLL for a desired diffraction order. The wave front W_b of the wave diffracted by the MLL is obtained by superposing the complex amplitudes $A^*(r_n, t)$ from all areas of the MLL. The intensity distribution at any point in the image plane can then be calculated from by propagating the wave front to the desired plane. In particular, the point spread function (PSF) can be obtained by calculating the intensity distribution in plane of best focus at a distance b^* from the rear surface of the MLL.

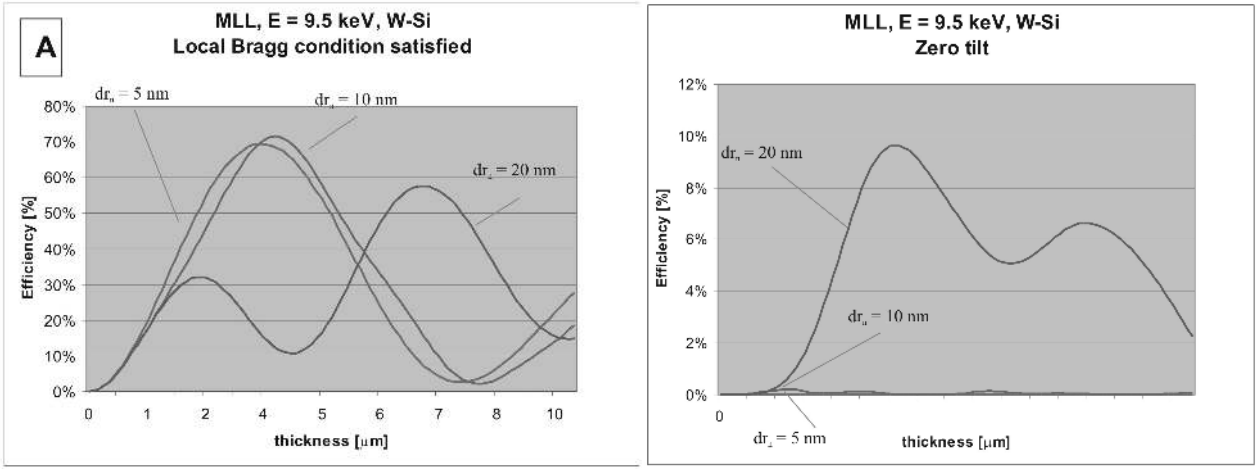

Figure 6: Local diffraction efficiency (LDE) of a MLL of alternating layers of W and Si for a photon energy of 9.5 keV. The LDE for areas of the MLL with zone width of 5 nm, 10 nm and 20 nm are indicated. This corresponds to a MLL with an outermost zone width of 5 nm and a central obstruction d_i of 25% of the effective aperture D_{eff}. Figure 6A shows the diffraction efficiency for a MLL where each zone is titled to an angle ψ that satisfies the local Bragg condition. The outer part of this MLL has a LDE of 70% at a thickness t of 4 μm, the inner part has a LDE of 32% at t = 2 μm, and a LDE of 18% t = 4 μm. Figure 6B shows the diffraction efficiency of a MLL where the zones are parallel to the optical axis. The Bragg condition is not satisfied, and the efficiency is significantly reduced. In the inner part of the MLL, the maximum LDE is 9% and quickly drops below 1%.

Figure 6 shows the local diffraction efficiency (LDE) of a 1-D MLL. The efficiency of a pair of 1-D MLLs is the product of the efficiency of the individual 1-D MLLs. Figure 6A represents calculations for a hypothetical ideal MLL, where the tilt angle varies with the zone number n to satisfy the local Bragg condition, $\theta_n = \sin^{-1}\left(\frac{\lambda}{4dr_n}\right)$. This is achieved by tilting each zone by an angle ψ_n with respect to the optical axis. For large demagnification, the tilt angle is given by $\psi_n \cong \frac{r_n}{2f}$. Figure 6B represents a MLL where the zones are not tilted ($\psi_n = 0$). If the Bragg condition is satisfied, a high LDE of 70% or above can be obtained for small zone widths between 5 and 10 nm. As the aspect ratio becomes smaller at larger zone width, the LDE becomes smaller, ultimately resembling that of a thin grating. If the zones are not tilted (Figure 6B), the local Bragg condition is not satisfied, and the LDE is significantly reduced even for large zone width of 20 nm. For smaller zone widths, the LDE drops well below 1%, and, in effect, most areas of the MLL do not contribute to focusing. In this case, significant phase effect are encountered that lead to destructive

interference in the focal plane and therefore loss of resolution. Note that for a practical MLL, the zones may all be tilted at a constant angle, which would give a case intermediate between these two extremes. Matching of the Bragg conditions for zones near the edge will most likely give optimum performance.

4. IMAGING PROPERTIES OF MULTILAYER LAUE LENSES

Figure 7 shows the ideal points spread function (PSF) of a MLL with various ratios $r_A = d_i/D_{eff}$. A constant LDE and absence of phase effects was assumed. For $r_A = 0$, the focal spot has a FWHM diameter of 5 nm, slightly smaller than the FWHM from a zone plate of corresponding outermost zone width dr_N. This is due to contributions from the corners of the MLL with smallest zone widths of $dr_N / \sqrt{2}$ (see Figure 4). As r_A becomes larger, the height of the side lobes increases quickly. For $r_A = 0.5$, the peak height of the side lobes corresponds to the half maximum of the central focus, and the resolution is effectively reduced to 33% of the design value. This should be compared to a zone plate, where $r_A = 0.5$ is often used in scanning microscopy, and the increase on the intensity of the side lobes affects background ratios but does not influence the spatial resolution significantly. It is therefore important, both from consideration of area ratio (Table 1), and from the imaging properties, that the MLL have a small central obstruction with $r_A \sim 0.25$. Conversely, this means that approx. 75% of the effective MLL aperture D_{eff} has to be covered with multilayer structures.

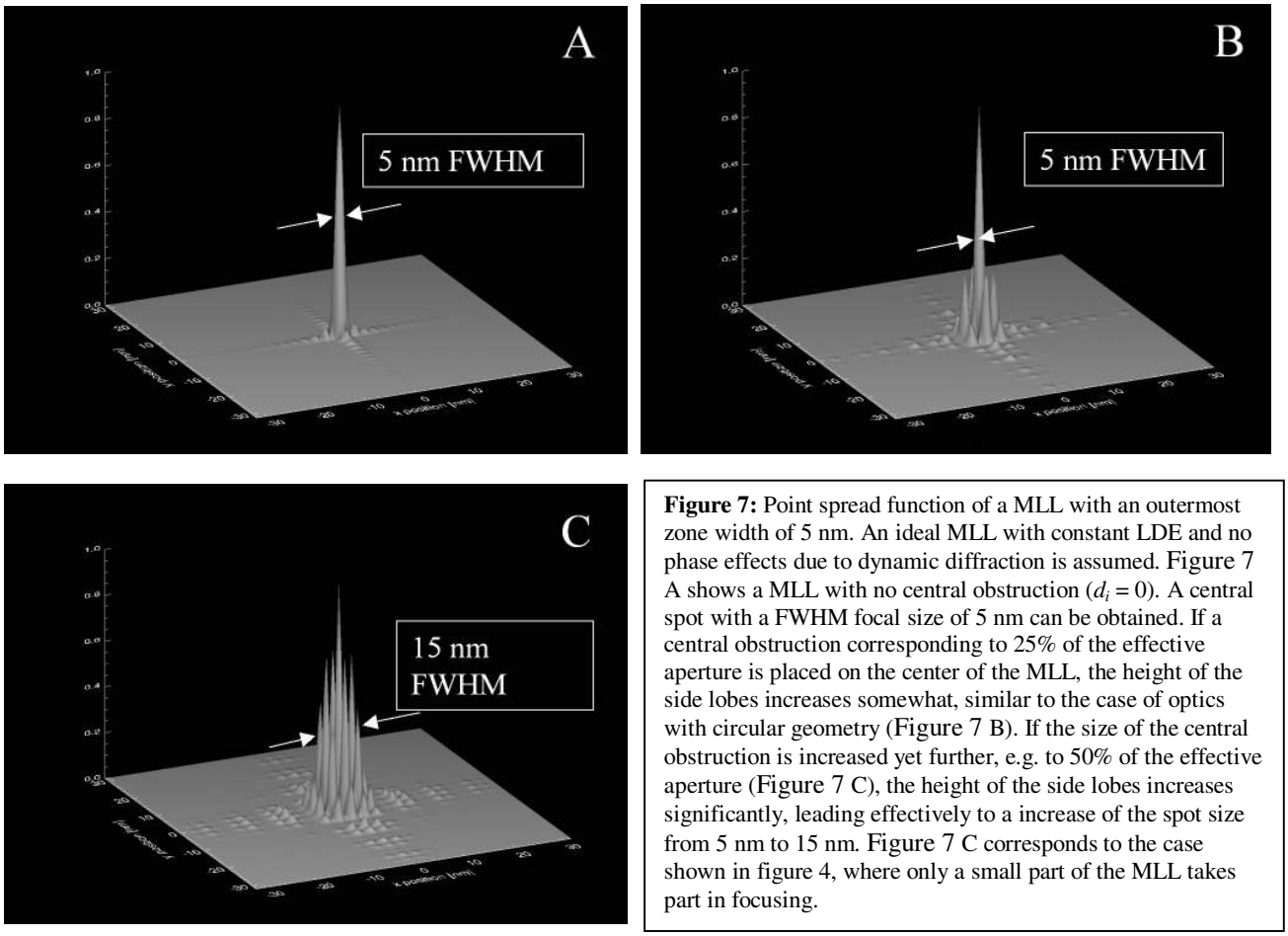

Figure 7: Point spread function of a MLL with an outermost zone width of 5 nm. An ideal MLL with constant LDE and no phase effects due to dynamic diffraction is assumed. Figure 7 A shows a MLL with no central obstruction ($d_i = 0$). A central spot with a FWHM focal size of 5 nm can be obtained. If a central obstruction corresponding to 25% of the effective aperture is placed on the center of the MLL, the height of the side lobes increases somewhat, similar to the case of optics with circular geometry (Figure 7 B). If the size of the central obstruction is increased yet further, e.g. to 50% of the effective aperture (Figure 7 C), the height of the side lobes increases significantly, leading effectively to a increase of the spot size from 5 nm to 15 nm. Figure 7 C corresponds to the case shown in figure 4, where only a small part of the MLL takes part in focusing.

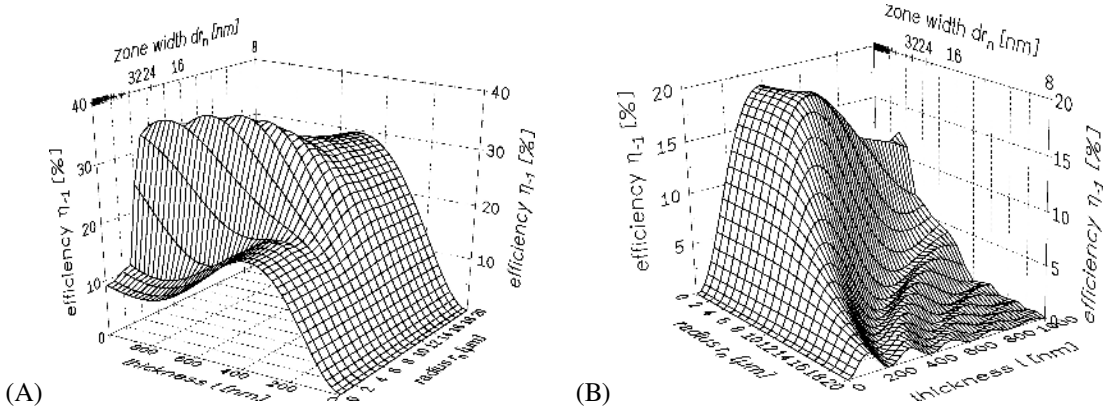

(A) (B)

Local diffraction efficiency in volume zone plates

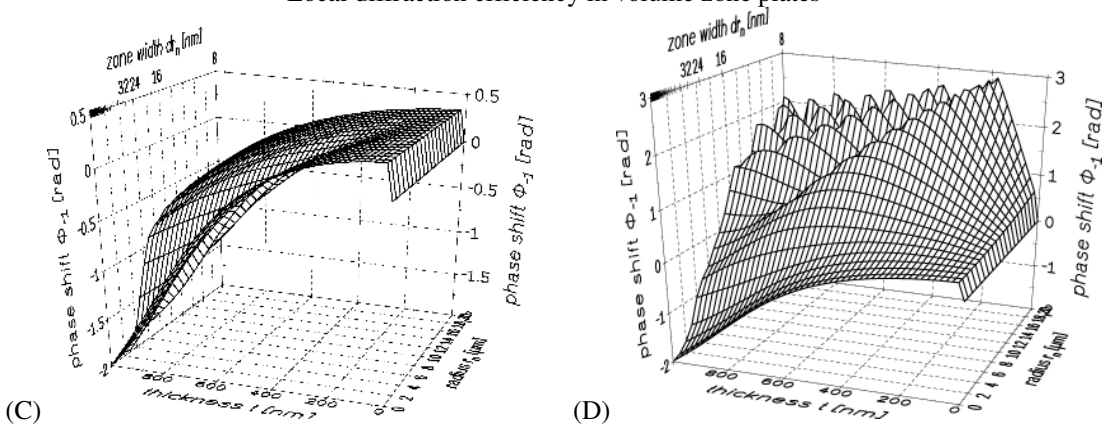

(C) (D)

Net phase shift of in volume zone plates

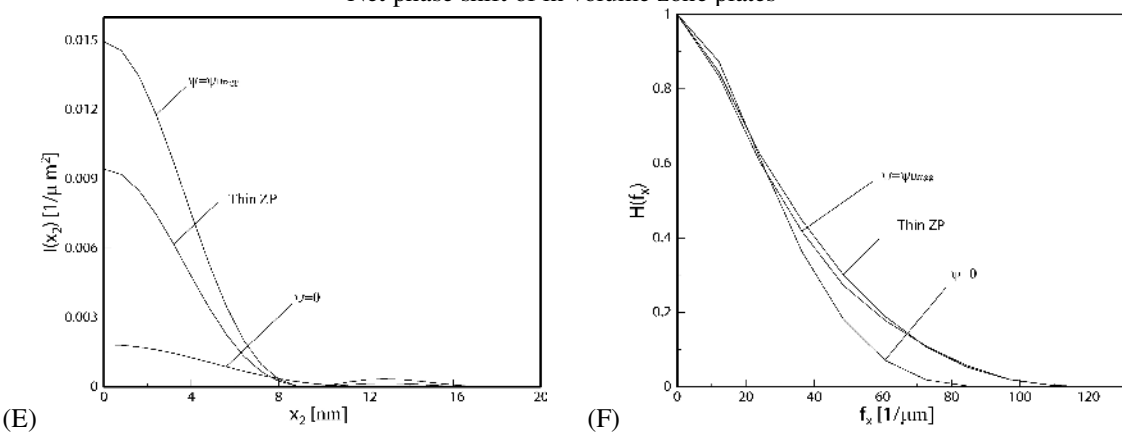

(E) (F)

Point spread function and modulation transfer function of volume zone plates.

Figure 8: Comparison of LDE, phase shifts and resulting optical transfer function for a volume zone plate. As an example, the diffraction properties of a zone plate of germanium with an outermost zone width of 8 nm at a photon energy of 8 keV are shown. Similar properties are encountered for a MLL with comparable optical constants. Figure 8A and B show the LDE for a FZP with zones that are tilted to satisfy the local Bragg condition (A), and for a FZP with untilted zones (B). One axis shows the radius of the FZP and the corresponding zone width, the second axis shows the thickness of the zones. Transition from "thin grating" diffraction to dynamic diffraction occurs for zone width of approximately 15 nm. Figure 8C and D show the corresponding net local phase shift Φ, which is calculated from the imaginary part of the complex amplitude $A^*(r_n, t)$, after extracting the fast oscillating part ~ $exp(ikz)$ of the electromagnetic field; Φ is a measure of radial differences in phase shift due to changes in d-spacing. If Φ is radially constant, waves diffracted by the center of the FZP experience the same phase delay as waves diffracted in the outer areas and interfere constructively in the focal spot. If Φ

varies significantly over the radius, different parts of the FZP interfere out of phase in the focal spot, and constructively elsewhere in the focal plane. This leads to a reduction in resolution. Figure 8E and F are the PSF and the MTF of the FZP. The PSF is calculated by propagating the wave front W_b into a plane of best focus and evaluating it along a line in that plane. The MTF is obtained by Fourier transform.

Figure 7 represents the ideal imaging properties of a MLL. However, both changes of the efficiency (see Figure 6) and changes of the phase are encountered in volume diffraction and will have to be convoluted with the point spread function (PSF) of the ideal MLL. As an example of the full diffraction properties encountered in a MLL, we discuss diffraction properties of a zone plate of germanium with an outermost zone width of 8 nm. The graphs in Figure 8 summarize these properties: Figure 8 (A) and (B) show the a radial increase in LDE if the Bragg condition is locally satisfied and a significant reduction for zero tilt, similar to the graphs shown in Figure 6. Figure 8 (C) and (D) show the effects that deviations from the Bragg condition have on the phase of the diffracted wave front. If the Bragg condition is satisfied ($\psi = \psi_B$, graph C), the net phase has only small radial changes. No destructive interference in the focal point is observed. Accordingly, the PSF ($\psi = \psi_B$, graph E) has the same FWHM diameter as the ideal case of a thin FZP, while the integrated intensity is higher, owing to the higher efficiency in the outer areas. The modulation transfer function (MTF) in this case closely matches that of the thin FZP, as expected. If the Bragg condition is not satisfied, ($\psi = 0$, graph D), radial changes of Φ on the order of π are encountered, leading to destructive interference in the image plan. This is reflected in the widened PSF ($\psi = 0$, graph E), and significantly reduced cutoff frequency in the MTF ($\psi = 0$, graph F).

The graphs in Figure 6 and Figure 8 represent imaging of a point source on the optical axis. In Figure 6A, Figure 8A and C, the local Bragg condition is satisfied for this on-axis point. When imaging an off-axis point in a full-field geometry, deviations from the Bragg condition are encountered even if the Bragg condition is satisfied for the point on-axis, and effects such as shown in Figure 6B, Figure 8A and Figure 8C will be encountered. The image of off-axis points therefore suffers reduced contrast and significant aberrations. High-resolution diffraction optics with nanometer resolution are therefore well suited as focusing systems, as needed in scanning microscopes and microprobes but not for full-field imaging.

5. THEORETICAL LIMIT OF THE APPROACH

There has been some discussion recently about the ultimate resolution limit for x-ray optics.[22,23] Bergemann et al. state that a universal resolution limit of approximately 10 nm applies to all x-ray optics.[22] They arrive at that statement by incorrectly generalizing results obtained for the near field behind an individual wave guide to the far-field distribution of a FZP. Kurokhtin et al. correctly obtains aberrations leading to a resolution limit of approximately 10 nm in the case of a zone plate that does *not* satisfy the Bragg condition but do not provide a calculation of the focal spot size for a zone plate with properly tilted zones.[23] While we do not undertake to address the question of the ultimate resolution limit of diffractive x-ray optics here, we wish to quantify the theoretical limit of the model presented here. Locally one-dimensional N-wave coupled wave theory is valid if (i) the optical constants are such that $\delta, \beta << 1$, and (ii) the thickness of the ZP or MLL satisfies $t << f$. These conditions are well satisfied for FZPs and MLLs with an outermost zone width of few nm and photon energies of 10 keV and above. Reconstruction of the wave field of a zone plate with an outermost zone width of 8 nm (Figure 8) has demonstrated that, if the Bragg condition is locally satisfied, the point spread function and modulation transfer function correspond to those of a thin lens with the same numerical aperture. In fact, due to increased LDE in the outer areas of such an optic, contrast transfer at high spatial frequencies is somewhat better than for an ideal lens, and the total diffraction efficiency is significantly higher.

To evaluate the resolution limit of dynamically diffracting focusing optics, such as high-resolution zone plates and MLLs for zone width smaller than a few nanometers, a more rigorous approach of coupled wave theory (or other approaches, such as coupled mode theory) has to be employed. In particular, second order derivatives have to be taken into account, as performed by Schneider,[24] and a 2-dimensional approach has to be used in place of the locally one-dimensional approach. This will allow one to take into account curvature of the individual zones, which will lead to a small change of d-spacing between the front and the back surface of the diffracting optics.

6. SUMMARY

Multilayer Laue lenses offer a technical path towards a highly efficient, true nanometer focusing system for hard x-rays. High local diffraction efficiencies for a 1-D MLL of 70% are possible, corresponding to a total efficiency of 50% of a 2-D MLL. Deposition of 75% of the effective aperture with multilayer structures must be achieved to reduce the height of secondary maxima in the focal plane, and to achieve the spatial resolution given by the numerical aperture of the MLL. The total focusing efficiency of a MLL is comparable to that of a zone plate with similar parameters. The MLL approach is particularly well suited to manufacturing high-resolution x-ray optics for use at high energies. Sectioning of the graded period multilayer becomes easier with increased thickness; the focal length and thereby the working distance become larger with increasing energy, and the required tilt angles become smaller.

ACKNOWLEDGMENTS

This work was supported by the U. S. Department of Energy, Office of Sciences, Office of Basic Energy Sciences, under Contract No. W-31-109-Eng-38. One of the authors (H.C.K.) also acknowledges support from Korea Science and Engineering Foundation (KOSEF) by the Post-doctoral Fellowship Program. We wish to thank Henry Chapman and Saša Bajt for useful discussions and for providing multilayers for our experimental efforts.

REFERENCES

1. J. Kirz, *J.,Opt. Soc. Am.* **64**, (1977), p. 301-309.
2. M. Peuker, *App. Phys. Lett.* **78** (15), (2001) pp. 2208-2210.
3. R.Divan, D.C.Mancini, N.Moldovan, B.Lai, L.Assoufid, Q.Leonard, F.Cerrina, *Proceeding SPIE* **4783**, Optical Science and Technology, Seattle 7-10 July, 2002, pp. 82-91.
4. A. A. Krasnoperova, J. Xiao, F. Cerrina, E. Di Fabrizio, L. Luciano, M. Figliomeni, M. Gentili, W. Yun, B. Lai, E. Gluskin. *J. Vac. Sci Techn. B* **11** (6), (1993), p. 2588-2591.
5. XRADIA Inc., http://www.xradia.com/pro_zpl.htm
6. B. D. Harteneck et. al., *Journ. Vac. Soc. B* (2004).
7. R.M. Bionta, K.M. Skulina, J. Weinberg, *App. Phys. Let.* **64**, 945 (1994).
8. S. Tamura et al., *J. Synchrotron Rad.* **9**, 154 (2002)
9. N Kamijo et al., *Rev. Sci. Instrum*. **74**, 5101 (2003); S. Tamura et al., *J. Synchrotron Rad.* **9**, 154 (2002)
10. B. Kaulich, Ph.D thesis, Göttingen, 1996.
11. A. Düvel, Ph.D. thesis, Göttingen, 1999.
12. H. C. Kang, G. B. Stephenson, C. Liu, R. Conley, A. T. Macrander, J. Maser, S. Bajt, and H. N. Chapman, *Proc. SPIE* **5537** (2004)
13. M. Born, E. Wolf. *Principles of Optics*. Sixths Edition, Pergamon Press**,** (1987).
14. D.T. Attwood, *Soft x-rays and Extreme Ultraviolet Radiation: Principles and Applications.* Cambridge University Press, (2000).
15. R. R. A. *Syms Practical Volume Holography*. Clarendon Press, Oxford 1990
16. T. K. Gaylord, M. G. Moharam. *Proc. IEEE* **73**, (1985), 894 – 936.
17. R.Magnusson, T.K.Gaylord. *J. Opt. Soc. Am.* **68**, (1978), 1777—1779.
18. L.Solymar, D.J.Cooke. *Volume Holography and Volume Gratings*. Academic Press, London, New York, Toronto, Sydney, San Francisco 1981.
19. J. Maser, G. Schmahl, *Opt. Comm.* **89**, (1992), 355-362.
20. R.R.A. Syms,Solymar, *J. Opt. Soc. Am*. **72**, (1982), 179-186.
21. R.R.A. Syms, L.Solymar. *Appl.Opt*. **21**, (1982), 3263-3268
22. C. Bergeman, H. Keymeulen, and J. F. van der Veen. *Phys. Rev. Let.* **91**, (2003), 204801/1 – 204801/4.
23. A. N. Kurokhtin, A. V. Popov, *J. Opt. Soc. Am. A* **19,** No 2, (2002), 315-324.
24. G. Schneider, *App. Phys. Lett*. **71**, No.16, 20. (1997), 2242-2244.